



Cite this: DOI: 10.1039/c8nj05939j

Novel phenyl-substituted pyrazinoporphyrazine complexes of rare-earth elements: optimized synthetic protocols and physicochemical properties†

A. D. Kosov,^a T. V. Dubinina,^b N. E. Borisova,^c A. V. Ivanov,^a K. A. Drozdov,^a S. A. Trashin,^d K. De Wael,^d M. S. Kotova^a and L. G. Tomilova^{ab}

Novel synthetic protocols based on both template and multi-step methods were developed for phenyl-substituted pyrazinoporphyrazine complexes of rare-earth elements (Y, Eu, Gd, Dy, Er and Lu). *p*-Hydroquinone was employed as a reaction medium and as a reducing agent in the process of porphyrazine macrocycle formation. Both thermal and microwave irradiation techniques were successfully applied for activation of the template macrocyclization process. An alternative multi-step approach involving the initial stage of free-base ligand formation was realized for the lutetium compound. The target complexes were identified by high-resolution mass spectrometry, infrared spectroscopy and nuclear magnetic resonance (NMR) spectroscopy. Electrochemical behavior in solution and UV-vis absorbance in solutions and films were studied as well. Shifts in the position of the Q band and oxidation–reduction potentials in comparison with corresponding phthalocyanine analogues were noticed. Using the IR absorption spectra recorded in the temperature range of 170–300 K, the position of the Fermi level of -4.7 ± 0.1 eV and a characteristic energy diagram were obtained for the erbium complex.

Received 22nd November 2018,
Accepted 22nd January 2019

DOI: 10.1039/c8nj05939j

rsc.li/njc

Introduction

Annulation of the porphyrazine macrocycle by four electron-deficient pyrazine moieties leads to the appearance of enhanced nonlinear optical properties,^{1,2} n-type conductivity,³ and interesting photochemical and photophysical properties.^{4–6} Similar to phthalocyanine complexes, the structure of pyrazinoporphyrazines can be modified by incorporation of peripheral substituents and variation of the central metal. Porphyrazine and phthalocyanine single-decker complexes of lanthanides can be used as building blocks in the synthesis of sandwich-type architectures,^{7–15} as well as for the creation of hybrid materials.^{16,17} In addition, lanthanide(III) monophthalocyaninates usually show good solubility and decreased aggregation tendency due to the steric effect of an axial ligand and high accessibility of the central lanthanide ion to solvation. Despite the promising

properties and unique structural features, only little attention has been paid to pyrazinoporphyrazine complexes of rare-earth elements (REE). Kobayashi *et al.* described *tert*-butyl substituted single- and double-decker lutetium pyrazinoporphyrazines.¹⁸ Their octa-substituted analogues were synthesized by two other groups, but the complexes were identified only by IR spectroscopy and elemental analysis.^{19,20} Thus, developing an effective synthesis and characterization of new pyrazinoporphyrazine complexes of REE is an important task.

The present paper focuses on the development of effective techniques to synthesize substituted REE tetrapyrazinoporphyrazine complexes. 5,6-Diphenylpyrazine-2,3-dicarbonitrile was chosen herein as a model compound for the development of synthetic approaches to pyrazinoporphyrazines due to its high availability. Additionally, we previously showed^{21,22} that the incorporation of phenyl-groups onto the macrocycle periphery can increase intramolecular interactions and improve the conductivity of the target complexes in films.

Results and discussion

The most convenient synthetic approach to initial 5,6-diphenylpyrazine-2,3-dicarbonitrile **1** includes the reaction between benzil and diaminomaleonitrile in the presence of different

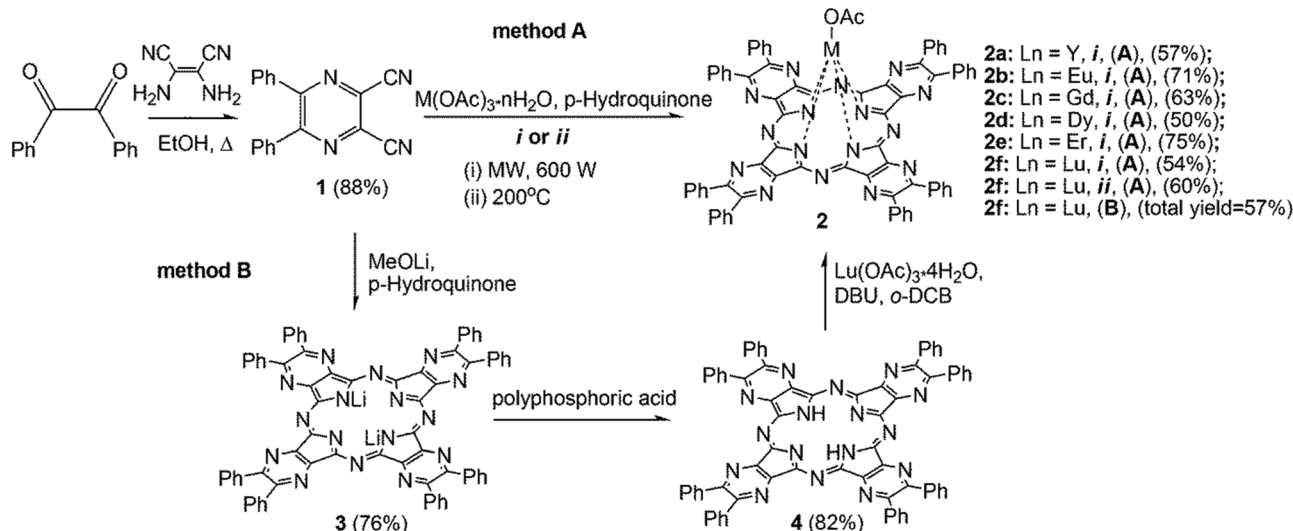
^a Department of chemistry, Lomonosov Moscow State University, 119991 Moscow, Russian Federation. E-mail: dubinina.t.vid@gmail.com

^b Institute of physiologically Active Compounds, Russian Academy of Science, 142432 Chernogolovka, Moscow Region, Russian Federation

^c A.N. Nesmeyanov Institute of Organoelement Compounds Russian Academy of Science, 28 Vavilov Str., 119334 Moscow, Russian Federation

^d AXES research group, University of Antwerp, 2020 Antwerp, Belgium

† Electronic supplementary information (ESI) available. See DOI: 10.1039/c8nj05939j



Scheme 1 Synthesis of phenyl-substituted pyrazinoporphyrazine complexes **2a–f**.

acids and ethanol.^{5,23,24} In the current work, compound **1** was obtained, using ethanol as a solvent (Scheme 1).

It was earlier demonstrated²⁰ that template synthesis of unsubstituted and tetra-*tert*-butylsubstituted pyrazinoporphyrazine complexes of lanthanides in a melt of the initial nitrile gives the target compounds in 10–30% yield. Our attempts to obtain octaphenyl-substituted porphyrazine REE complexes **2** from nitrile **1** in melt or in solutions of high-boiling alcohols (isoamyl alcohol, and *n*-octanol) were unsuccessful. Instead, we found that formation of compounds **2a–f** takes place in a melt of *p*-hydroquinone. Since macrocyclization of **1** includes the reduction stage, we decided to use *p*-hydroquinone as a reducing agent and at the same time the reaction medium. *p*-Hydroquinone was earlier utilized in the synthesis of phthalocyanines.^{25,26} However, the target phthalocyanines were synthesized in low yields (about 20%). In the present study, *p*-hydroquinone was used for the first time in the synthesis of porphyrazines. Noteworthy, the yields of the target complexes were high, sometimes reaching 75%. On the example of lutetium complex **2f**, we also showed that both thermal and microwave energy can be successfully employed for heating the reaction mixture with nearly equal effectiveness (Scheme 1).

For comparison, a multi-step approach through the intermediate formation of the porphyrazine ligand was applied on the example of compound **2f** (Scheme 1). In order to avoid harsh demetallation by a strong (sulfuric) acid in the synthesis of porphyrazine ligand **4** as commonly used in demetallation of Mg phthalocyanines and their analogues,^{8,16,21,23,27} we used dilithium salt **3**, which was further demetallated by freshly obtained polyphosphoric acid. The following insertion of lutetium was performed in boiling *o*-DCB in the presence of DBU as a base. The total yield of the three stages (lithium salt formation, demetallation, and metalation) of the multi-step approach is similar to that of the one-step procedure (Scheme 1).

All the obtained compounds were characterized by MALDI TOF mass spectrometry, including high-resolution spectra (Table 1).

Table 1 High-resolution MALDI TOF/TOF mass spectrometry data

Compound (Molecular formula)	Ion	Mass calculated	Mass found
2a (C ₇₉ H ₄₆ N ₁₆ O ₄ Y)	[M-OAc + DHB] ⁺	1371.2946	1371.2944
2b (C ₇₂ H ₄₀ EuN ₁₆)	[M-OAc] ⁺	1281.2834	1281.2746
2c (C ₇₂ H ₄₀ GdN ₁₆)	[M-OAc] ⁺	1286.2863	1286.2749
2d (C ₉₂ H ₅₄ DyN ₁₈ O ₆)	[M-OAc + 2CHCA] ⁺	1670.3765	1670.3651
2e (C ₉₂ H ₅₄ ErN ₁₈ O ₆)	[M-OAc + 2CHCA] ⁺	1672.3777	1672.2586
2f (C ₇₉ H ₄₆ LuN ₁₆ O ₄)	[M-OAc + DHB] ⁺	1457.3296	1457.3768

In the case of REE complexes **2a–f**, ionization is accompanied by cleavage of axial acetate. Moreover, in the case of more rigid small ions (Dy³⁺, Er³⁺, Lu³⁺ and Y³⁺) the further formation of adducts with the matrices (O-ligands) was observed under laser ionization.

As an example, the mass-spectrum of gadolinium complex **2c** is shown in Fig. 1. The isotopic pattern of the molecular ion agrees well with the calculated pattern.

In FT-IR spectra of complexes **2a–f** (Fig. 2 shows the spectrum of dysprosium complex **2d** as a representative example), skeletal vibrations of the pyrrole and pyrazine fragments occupy the region from 1375 to 1635 cm⁻¹. Stretching vibrations of CH from phenyl groups are observed at 3054–3066 cm⁻¹ and those for the axial acetate can be seen at 2850–2981 cm⁻¹. The bands at 1282–1446 cm⁻¹ and 1512–1635 cm⁻¹ were assigned to C–O and C=O vibrations, respectively. The same values were reported for acetates in the literature²⁸ and for perchlorinated phthalocyanines of lanthanides bearing acetate counter-ions, which were reported by us earlier.¹⁶

In the case of porphyrazine ligand **4**, stretching vibrations of NH groups are observed at 3288 cm⁻¹ (Fig. S2, ESI[†]). The same values were observed for phthalocyanine ligands.^{16,29}

In this work, pyridine-*d*₅ was chosen as a solvent for the NMR measurements due to its ability to coordinate with a central metal ion, which allows the suppression of the aggregation of the target complexes and improves their solubility. In the case of diamagnetic complexes of yttrium **2a** and lutetium

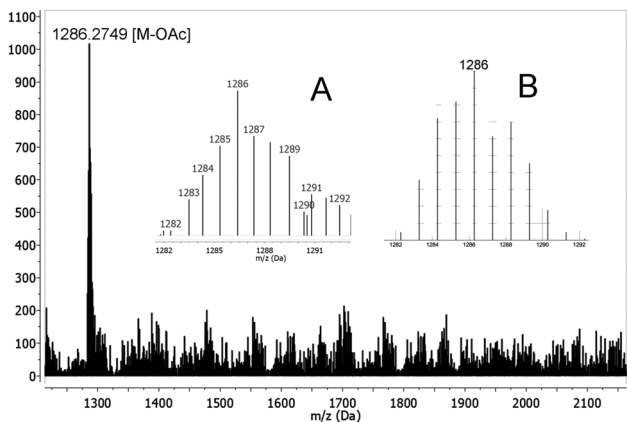


Fig. 1 MALDI-TOF mass spectrum of **2c**, isotopic pattern of the molecular ion (inset A) and simulated MS pattern of the molecular ion (inset B).

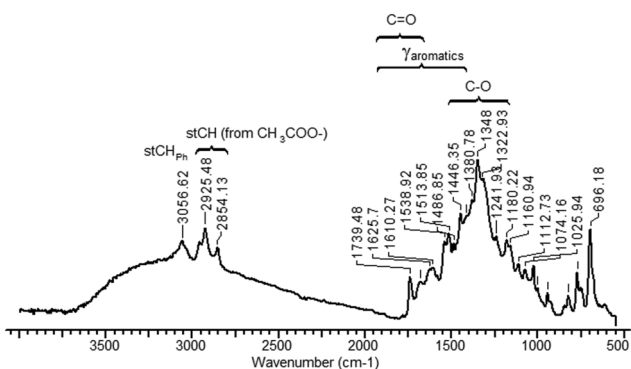


Fig. 2 FT-IR spectra of dysprosium complex **2d** in ZnSe.

2f, the signals of phenyl protons occupy the same region of the spectra as it is observed for their precursor – 5,6-diphenylpyrazine-2,3-dicarbonitrile.

The NMR data of compounds **2** with paramagnetic REE are of special note. Despite the fact that the lanthanide induced shifts in paramagnetic REE monophthalocyanines have been studied widely,^{25,30–32} the NMR spectra of porphyrazine complexes with paramagnetic REE have not been investigated previously. The effect of the paramagnetic nature of europium and erbium ions manifests in a downfield shift of the phenyl proton signals for compounds **2b** and **2e**, respectively, compared to analogues with diamagnetic REE (**2a** and **2f**) (Fig. 3 and Fig. S1, ESI[†]). The largest chemical shift value (21.70 ppm) was detected for erbium complex **2e** (Fig. 3B). The assignment of signals in the ¹H NMR spectrum of europium complex **2b** was made using the COSY technique (Fig. S1, ESI[†]). It was shown, that the most downfield shifted signals at 7.96 and 7.88 ppm most likely can be assigned to *ortho* protons of phenyl groups.

The opposite upfield shift of the signals of aromatic protons up to –26.88 ppm was observed for dysprosium complex **2d**.

For example, α -protons of the phthalocyanine macrocycle in erbium phthalocyaninate lie at 20–40 ppm,^{25,30,32} while the signals of α -protons for unsubstituted dysprosium monophthalocyaninate

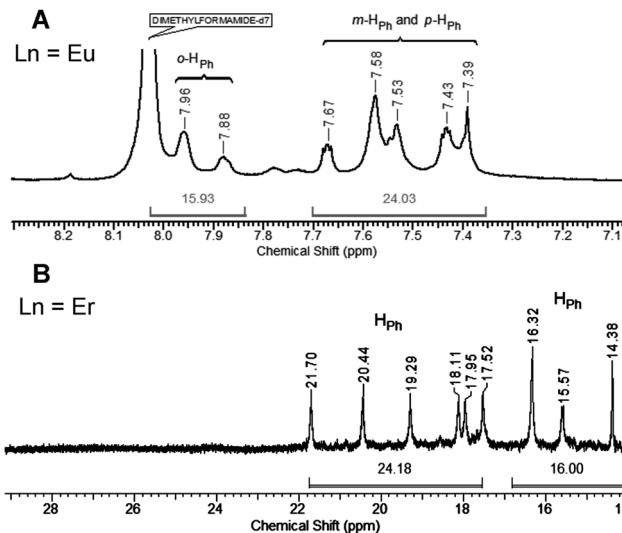


Fig. 3 ¹H NMR spectra of complexes **2b** (A) and **2e** (B) in [D₅]Py.

lie near –20 ppm.³⁰ In our case, a weaker effect of the paramagnetic REE apparently results from a larger distance between peripheral phenyl groups and the central REE ion in comparison to the reported data for α -protons of REE phthalocyaninates. As expected, the Gd analogue is NMR silent in [D₅]Py and [D₈]THF due to the strong paramagnetic nature of the Gd³⁺ ion.^{33,34}

In the UV-vis spectra of target lanthanide complexes **2a–f**, two absorption bands are observed: B band (348–358 nm) and Q band (663–665 nm). Due to the lower orbital symmetry and corresponding splitting of the LUMO,³⁵ the porphyrazine ligand **4** possesses two Q bands at 639 and 672 nm (Fig. 4A). As it was presented earlier for lanthanide(III) monophthalocyaninates, the lanthanide ion's nature does not influence the Q band position.²¹ In comparison with phenyl-substituted phthalocyanine complexes a hypsochromic shift of the Q band of about 30 nm is observed.³⁶

The UV-vis spectra were measured for erbium complex **2e**, in a thin film and in poly(methyl acrylate) film, that were deposited from a pyridine solution on a glass substrate by the drop casting method (Fig. 4B). Due to the aggregation effect, an increase of absorption intensity in the vibrational satellite area (582 nm) was observed indicating H-type aggregation, while a shoulder appeared near 740 nm implying formation of J-type aggregates. In poly(methyl acrylate) film, a polymeric matrix prevents strong aggregation of the porphyrazine molecules. It resulted in almost similar Q band positions for the dilute solution (663 nm) and polymeric film (665 nm) and the absence of intensive absorption at 582 nm.

Information regarding the energy spectrum for erbium complex **2e** was obtained from the current–voltage (*I–V*) characteristics and temperature evolution of the IR spectra.

For the **2e** film the *I–V* dependence for the Ag–active layer–Ag structure is linear (Fig. 5, inset), which indicates the absence of an energy barrier at the boundary of the active layer and Ag contact. This is possible when the positions of the Fermi levels in both materials are close and while the Fermi level in the

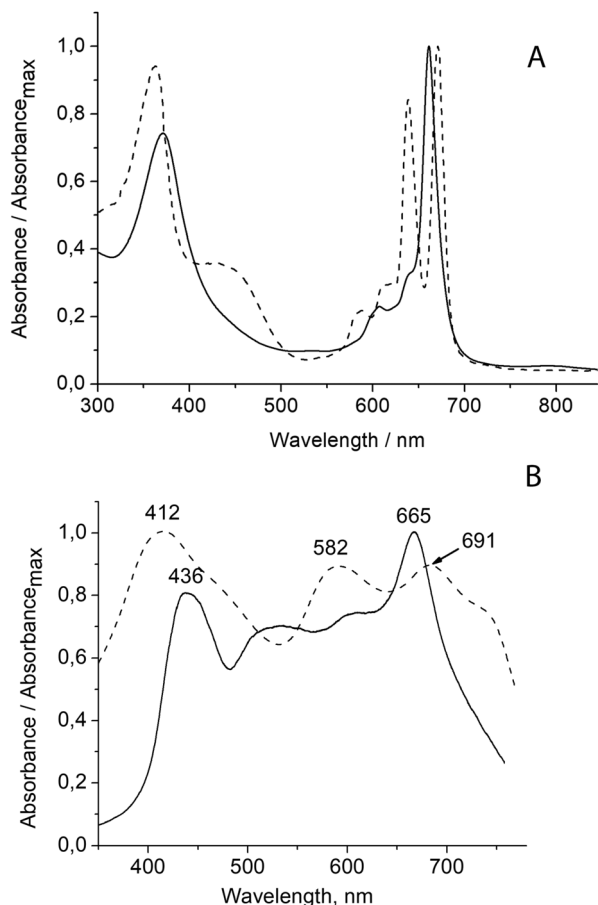


Fig. 4 UV-vis spectra of erbium complex **2e** (solid line) and porphyrazine ligand **4** (dashed line) in CHCl_3 (A). UV-vis spectra of erbium complex **2e**, in a thin film (solid line) and erbium complex **2e** in poly(methyl acrylate) film (dashed line) (B).

active layer lies close to the LUMO level.³⁷ It is established that the Fermi level in erbium complex **2e** film lies at -4.3 ± 0.1 eV; the LUMO level lies at or within 0.5 eV above the Fermi level.

The I - V curve for the ITO-active layer (**2e**)-Ag structure in the dark is non-linear with the activation barrier determined by the ITO-active layer boundary (Fig. 5). Illumination at wavelengths corresponding to the B and Q band in the absorption spectra (Fig. 4B) leads to the higher current values and linearization of the I - V curves. Since the Ag-ITO contact does not demonstrate such a behavior, the observed change in the curves should be associated with the active layer. It can be explained by the change in the activation energy to the mobility threshold due to the generation of photoexcited charge carriers and change in the position of the Fermi level in the active layer. Thus, the B and Q band absorption (Fig. 4) should be associated with the photoexcitation of electrons to the LUMO level from the levels lying 3.5 and 1.9 eV below the LUMO. Together with the absence of other absorption peaks besides the B and Q bands (Fig. 4), this result suggests the existence of a single energy level lying at or within 1 eV interval above the Fermi level. This level is already determined as the LUMO level.

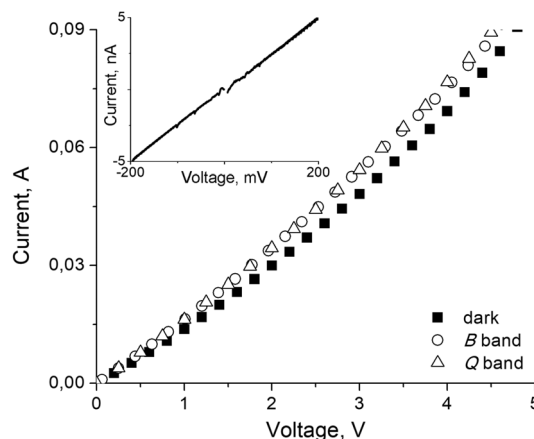


Fig. 5 I - V curves for the ITO-active layer (**2e**)-Ag sandwich structure in the dark (closed symbols) and under illumination with the wavelengths corresponding to the B band and Q band in the optical absorption spectra (open symbols). The inset shows the I - V curve for the Ag-active layer (**2e**)-Ag coplanar structure.

For **2e** film the temperature evolution of the IR transmittance in the 2000 – 8000 cm^{-1} wavenumber interval demonstrates significant changes only for 3100 – 3600 cm^{-1} (Fig. 6).

This behavior can be attributed to a change in the population of the energy levels. With temperature decrease the electron population at the LUMO level decreases substantially; the increase in absorption is due to the optical excitation of electrons to the LUMO from the lower-lying levels. To obtain the exact position of the LUMO level a simple model was used, where transmittance is calculated as $C - A \times f(E, T) \times (1 - f(E + dE, T))$, where constants C and A were considered temperature-independent, and $f(E, T)$ and $f(E + dE, T)$ followed the Fermi-Dirac distribution.³⁸ The value of dE was obtained from the position of the local minimum in Fig. 6 and amounted to 0.4 eV. These estimations show that the LUMO level in **2e** film lies 0.3 eV above the Fermi level. In addition, the presence of an additional level, lying 0.1 eV below the Fermi level and not seen in the absorbance in the UV-vis spectral range is acknowledged. The obtained results are in good agreement with the data known from the literature.

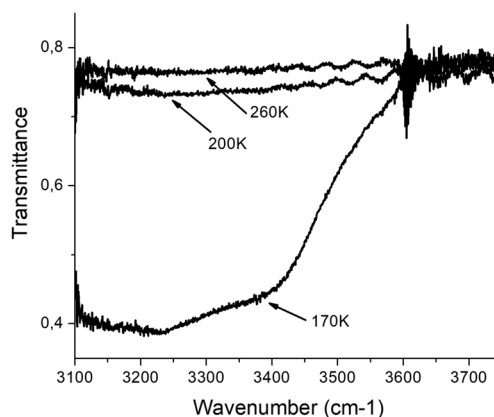


Fig. 6 Temperature evolution of the IR spectrum for thin film of erbium complex **2e**.

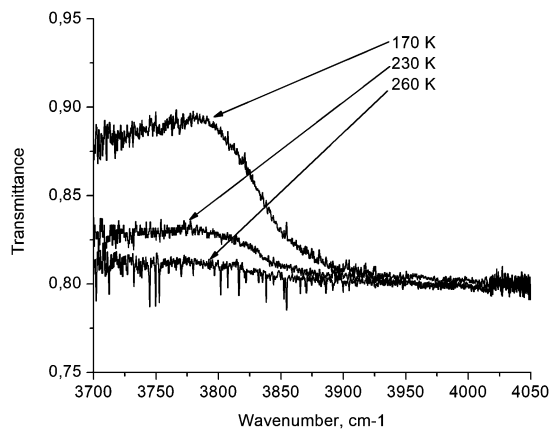


Fig. 7 Temperature evolution of the IR spectrum for erbium complex **2e** in poly(methyl acrylate) film.

For example, from the concentration of charge carriers for similar materials,³⁹ it follows that the LUMO should lie 0.2–0.4 eV above the Fermi level.

For erbium complex **2e** in poly(methyl acrylate) film the temperature evolution of the IR transmittance in the 2000–8000 cm^{-1} wavenumber interval demonstrates significant changes for 3700–4200 cm^{-1} (Fig. 7).

In order to analyze the curves, the same model was used with the transition of electrons from the lower-lying level to the higher-lying level and the evolution of the population of these levels with a change in temperature. These estimations show that the LUMO level for erbium complex **2e** in poly(methyl acrylate) film lies 0.6 eV above the Fermi level. The excitation of electrons to the LUMO level is carried out from the level lying 0.14 eV above the Fermi level.

The qualitative difference in the temperature dependence of the transmittance (Fig. 6 and 7) can be explained from the position of the levels relative to the Fermi level. For the **2e** film (Fig. 6), electron excitation occurs from a level lying below the Fermi level. Its population varies little with temperature. The main contribution is provided by a decrease in the population of the LUMO level with temperature decrease. As a result, the excitation of electrons to the LUMO level proceeds more intensively and the transmittance decreases. For the erbium complex **2e** in poly(methyl acrylate) film (Fig. 7), both levels lie above the Fermi level. In this case, the main contribution is provided by a decrease in the population of the lower level with temperature decrease. The excitation of electrons from this level proceeds less intensively and the transmittance increases.

A significant difference in the spectral characteristics of pure film of **2e** and **2e** in poly(methyl acrylate) film is due to the aggregation effect. For the B and Q bands in the UV-vis spectral range (Fig. 4B), aggregation in the film leads to a shift of the local absorption maxima towards higher energies by 0.17 and 0.07 eV, respectively. This shift must be correlated with the simultaneous distortion of the LUMO level in k -space and the displacement of the LUMO position in terms of energy. The HOMO levels are significantly less affected and their energy values can be taken as aggregation independent⁴⁰ with the

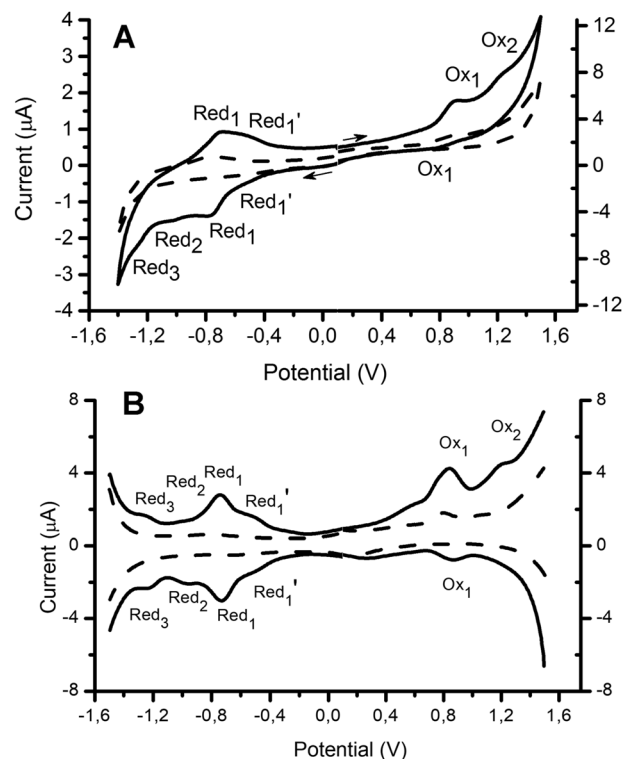


Fig. 8 CV (A) and SWV (B) of complex **2e** (1.2 mM) recorded at room temperature in pyridine containing 0.1 M TBABF₄. Dashed lines depict voltammograms of the background. Pt disk working electrode; CV scan rate, 0.1 V s⁻¹; SW modulation amplitude, 50 mV; frequency, 10 Hz; step potential, 5 mV.

previously introduced error of 0.1 eV. This allows construction of a characteristic energy diagram for the erbium complex **2e**.

The redox properties of erbium complex **2e** were investigated by cyclic (CV) and square wave (SWV) voltammetry (Fig. 8). Table 2 summarizes the found formal oxidation–reduction potentials. Since the central lanthanide ion in phthalocyanines (except Ce³⁺) does not change its oxidation state,^{41,42} all found redox processes for **2e** were referred to the pyrazinoporphyrazine macrocycle.

In total, three reductions and two oxidations were observed within the available potential window (–1.6 to +1.6 V). In the same conditions Fc⁺/Fc shows the formal potential of +0.610 V.

An additional peak (Red₁') at –0.51 V was attributed to strongly adsorbed one-electron reduced **2e** because of its peculiar behavior in CV at different scan rates (Fig. S3, ESI†).

The peak current of Red₁ was linearly proportional to the square root of the scan rate as expected for a diffusion controlled electrochemical process, while the peak Red₁' was noticeable only at the backward scan, and it became more pronounced at higher scan rates as expected for electrochemical processes complicated by adsorption. Moreover, electrochemistry of pyrazinoporphyrazines can be complicated by aggregation and coordination of pyridine.⁴³ Oxidation of analogous pyridinium-substituted pyrazinoporphyrazines in pyridine was not observed previously,⁴⁴ but two oxidations were found for analogous phenyl-substituted diazepinoporphyrazines in pyridine⁴⁵ at slightly lower potentials compared to **2e** (Table S1, ESI†).

Table 2 The oxidation–reduction potentials $E_{1/2}$ (V) for complex **2e** in pyridine. $E_{1/2}(\text{Fc}^+/\text{Fc}) = +0.610$ V

	Red ₃	Red ₂	Red ₁ ^a	Ox ₁	Ox ₂	$\Delta E_{\text{Red1-Ox1}}$
	$[\text{Ph}^{\text{st}}\text{TPyzPzLnOAc}]^{2-/3-*b}$	$[\text{Ph}^{\text{st}}\text{TPyzPzLnOAc}]^{1-/2-}$	$[\text{Ph}^{\text{st}}\text{TPyzPzLnOAc}]^{0/1-*}$	$[\text{Ph}^{\text{st}}\text{TPyzPzLnOAc}]^{1+*/0}$	$[\text{Ph}^{\text{st}}\text{TPyzPzLnOAc}]^{2+/1+*}$	
$E_{1/2}$	−1.24	−0.98	−0.74	+0.86	+1.20	1.60
$E_{1/2}$ vs. Fc^+/Fc	−1.85	−1.59	−1.35	+0.25	+0.59	1.60

^a An additional peak Red₁' at −0.51 V (−1.12 V vs. Fc^+/Fc) was observed. ^b $\text{Ph}^{\text{st}}\text{TPyzPz}$ = phenyl-substituted pyrazinoporphyrazine.

In comparison to phenyl-substituted phthalocyanines ($\text{Ph}^{\text{st}}\text{PcLuOAc}$, Table S1, ESI†) in *o*-DCB,²¹ the oxidation and reduction processes in **2e** are shifted towards higher potentials due to the electron-withdrawing effects of the four pyrazine fragments fused to the porphyrine macrocycle.^{46,47} As a consequence of the anodic shift, the third reduction Red₃ was observed for **2e** but it was not detected for $\text{Ph}^{\text{st}}\text{PcLuOAc}$ in the potential window of *o*-DCB. Similar to phthalocyanines, electron withdrawing and donating peripheral substituents can strongly affect the oxidation–reduction potentials as it is seen from comparison of octachloro- and octadodecyl-substituted pyrazinoporphyrazines.^{48,49} In this view, the eight phenyl groups should result in a strong electron donating effect that explains a cathodic shift in the reduction potentials compared to octa(2-(*N*-methyl)pyridiniumyl)- and octa(2-pyridyl)-substituted pyrazinoporphyrazines.^{44,50} The HOMO–LUMO gap calculated from the difference in the potentials of Red₁ and Ox₁ ($\Delta E_{\text{Red1-Ox1}} = 1.60$ V for **2e**) is rather the same as that for $\text{Ph}^{\text{st}}\text{PcLuOAc}$ in *o*-DCB (Table S1, ESI†),²¹ although about 10% increase in the band gap was previously predicted by DFT calculations for unsubstituted pyrazinoporphyrazines compared to phthalocyanines.⁴⁷

Taking into account all uncertainty factors, the experimental finding rather agrees with the theoretical prediction that the band gaps should lie close together for pyrazinoporphyrazines and phthalocyanines. Noteworthy, the bandgap of **2e** is about 0.24 V larger than the bandgap of phenyl-substituted diazepinoporphyrazines studied in the same solvent ($\Delta E_{\text{Red1-Ox1}} = 1.36$ V).⁴⁵

Experimental

Materials and methods

All reagents and solvents were obtained or distilled according to standard procedures. All reactions were monitored by TLC and UV/vis until complete disappearance of the starting reagents if not additionally specified. Thin-layer chromatography was performed using Merck Aluminium Oxide F₂₅₄ neutral flexible plates. The salts $\text{Y}(\text{OAc})_3 \times 4\text{H}_2\text{O}$, $\text{Eu}(\text{OAc})_3 \times 3\text{H}_2\text{O}$, $\text{Gd}(\text{OAc})_3 \times 4\text{H}_2\text{O}$, $\text{Dy}(\text{OAc})_3 \times 4\text{H}_2\text{O}$, $\text{Er}(\text{OAc})_3 \times 4\text{H}_2\text{O}$ and $\text{Lu}(\text{OAc})_3 \times 4\text{H}_2\text{O}$ were dried immediately before use for 4 h at 70 °C.

The synthesis under microwave irradiation was performed using a Samsung microwave oven. UV-vis absorption spectra were recorded on a ThermoSpectronic Helios- α spectrophotometer using quartz cells (1 × 1 cm). Matrix assisted laser desorption/ionization time-of-flight (MALDI-TOF) mass-spectra were taken on a Bruker Autoflex II mass spectrometer with 2,5-dihydroxybenzoic acid (DHB) or α -cyano-4-hydroxycinnamic

acid (CHCA) as the matrix. High-resolution MALDI mass spectra were obtained using a Bruker ULTRAFLEX II TOF/TOF instrument. ¹H and ¹H–¹H COSY NMR spectra were recorded on Bruker Avance 400 and Bruker Avance 600 spectrometers (400.13 and 600.13 MHz). Chemical shifts are given in ppm relative to SiMe_4 .

FT-IR spectra were obtained using an IR 200 ThermoNicolet spectrometer with a spectral resolution $\Delta\lambda = 4$ cm^{−1}.

Temperature evolution of the IR spectrum was investigated using a Bruker Vertex 70v spectrometer (spectral resolution, $\Delta\lambda = 4$ cm^{−1}) with an Oxford cryostat in a temperature range 300–170 K. *I*-*V* characteristics were measured using a Keithley 6430 Source Meter. Samples were fabricated in coplanar and sandwich geometry. An active layer was deposited on the substrates by drop casting from the solution in pyridine. The thickness of the active layer was about 2 μm (estimated by optical microscopy). For the coplanar geometry, a pair of silver contacts with a contact gap of 200 μm was used. For the sandwich geometry an ITO conducting layer on the glass substrate (lower contact) and a silver layer (upper contact) were used. The upper silver layer was formed using silver paste “Kontaktol”. Illumination of samples in the sandwich geometry was carried out from the ITO contact side (transparent in the visible spectral range) using a white light lamp and a MDR-206 monochromator.

Electrochemical measurements were performed using a Metrohm-Autolab 302N instrument. A platinum rod and double junction Ag/AgCl (1 M LiCl in ethanol) were used as a counter electrode and a reference electrode, respectively. A Pt disk electrode (BASi MF-2013, 1.6 mm in diameter) was used as a working electrode. Prior to use, the working electrodes were polished with abrasive paper (grit 400), cleaned in ultrapure water in an ultrasound bath and dried with compressed air. Ferrocene was used as an internal reference. Pyridine (dehydrated, SeccoSolv[®], Merck Millipore) containing 0.1 M tetrabutylammonium tetrafluoroborate (TBABF_4 , Sigma-Aldrich, for electrochemical analysis, $\geq 99.0\%$) was used as background electrolyte.

Synthetic procedures

5,6-Diphenylpyrazine-2,3-dicarbonitrile (1). Benzil (1.06 g, 5.00 mmol) and diaminomaleonitrile (0.54 g, 5.00 mmol) were refluxed in 100 mL ethanol for 6 h (TLC-control: SiO_2 , ethyl acetate : hexane (1 : 2)). Then the reaction mixture was cooled to room temperature. The resulting residue was filtered off, washed with cold $\text{C}_2\text{H}_5\text{OH}$ (3 × 30 mL) and dried at room temperature to give compound **1** (1.24 g, 88%). M.p. 244–246 °C (lit. 246 °C⁵¹). ¹H NMR (400.13 MHz, $[\text{D}_5]\text{Py}$) δ H ppm: 7.35–7.39, 7.43–7.47 and 7.65–7.67 (m, Ph).

Synthesis of phenyl-substituted pyrazinoporphyrazine complexes of rare-earth elements 2a–e

General procedure. 5,6-Diphenylpyrazine-2,3-dicarbonitrile **1** (0.20 g, 0.71 mmol), $\text{Ln}(\text{OAc})_3 \times n\text{H}_2\text{O}$ (0.36 mmol) and *p*-hydroquinone (0.16 g, 1.45 mmol) were taken in a glass tube. The resulting mixture was irradiated in a microwave oven (600 W) for 15 min. Then the reaction mixture was cooled to room temperature and a MeOH–H₂O (20 : 1 v/v) mixture was added. The precipitate was filtered and washed with H₂O, MeOH, and acetone.

[2,3,9,10,16,17,23,24-Octaphenyl-1,4,8,11,15,18,22,25-octaazaphthalocyaninato]yttrium acetate (2a). Yield 0.13 g (57%). MS (MALDI-TOF) *m/z*: 1354 ([M–OAc + DHB–OH]⁺, 100%), 1371 ([M–OAc + DHB]⁺, 90%). UV-vis λ_{max} (Py)/nm 350 (lg ϵ 4.43) and 663 (3.90). ¹H NMR (600.13 MHz, [D₅]Py) δ H ppm: 7.71 (16H, m, H_{Ph}), 7.76–7.79 (16H, m, H_{Ph}) and 7.86–7.92 (8H, m, H_{Ph}). IR (KBr): ν (cm^{–1}): 1319–1446 (C–O), 1375–1635 (γ pyrrole and pyrazine), 1512–1635 (C=O), 2833–2981 (st CH CH₃COO[–]), 3062 (st CH_{Ph}).

[2,3,9,10,16,17,23,24-Octaphenyl-1,4,8,11,15,18,22,25-octaazaphthalocyaninato]europium acetate (2b). Yield 0.17 g (71%). MS (MALDI-TOF) *m/z*: 1281 ([M–OAc]⁺, 85%), 1551 ([M–OAc + CCA + Na], 100%). UV-vis λ_{max} (Py)/nm 348 (lg ϵ 4.77) and 665 (4.54). ¹H NMR (600.13 MHz, [D₇]DMF) δ H ppm: 7.39–7.67 (24H, m, H_{Ph}) and 7.88–7.96 (16H, m, H_{Ph}). IR (KBr): ν (cm^{–1}): 1282–1381 (C–O), 1381–1539 (γ pyrrole and pyrazine), 1539–1630 (C=O), 2854–2931 (st CH CH₃COO[–]), 3055 (st CH_{Ph}).

[2,3,9,10,16,17,23,24-Octaphenyl-1,4,8,11,15,18,22,25-octaazaphthalocyaninato]gadolinium acetate (2c). Yield 0.15 g, (63%). MS (MALDI-TOF) *m/z*: 1286 ([M–OAc]⁺, 100%). UV-vis λ_{max} (Py)/nm 349 (lg ϵ 4.41) and 665 (4.23). IR (KBr): ν (cm^{–1}): 1319–1446 (C–O), 1377–1626 (γ pyrrole and pyrazine), 1512–1626 (C=O), 2854–2924 (st CH CH₃COO[–]), 3066 (st CH_{Ph}).

[2,3,9,10,16,17,23,24-Octaphenyl-1,4,8,11,15,18,22,25-octaazaphthalocyaninato]dysprosium acetate (2d). Yield 0.12 g (50%). MS (MALDI-TOF) *m/z*: 1670 ([M–OAc + 2CHCA]⁺, 10%), 1774 ([M–OAc + 2CHCA + *p*-hydroquinone]⁺, 100%). UV-vis λ_{max} (Py)/nm 358 (lg ϵ 4.70) and 665 (4.61). ¹H NMR (600.13 MHz, [D₅]Py) δ H ppm: –26.88–23.21 (8H, m, H_{Ph}), –20.96–12.11 (16H, m, H_{Ph}) and –10.40–4.30 (16H, m, H_{Ph}). IR (ZnSe): ν (cm^{–1}): 1323–1446 (C–O), 1381–1626 (γ pyrrole and pyrazine), 1514–1626 (C=O), 3056 (stCH_{Ph}), 2854–2925 (st CH CH₃COO[–]), 3056 (st CH_{Ph}).

[2,3,9,10,16,17,23,24-Octaphenyl-1,4,8,11,15,18,22,25-octaazaphthalocyaninato]erbium acetate (2e). Yield 0.18 g (75%). *m/z* (MALDI TOF) (%): 1407 ([M–OAc + *p*-hydroquinone]⁺, 80%), 1672 ([M–OAc + 2CHCA]⁺, 100%). UV-vis λ_{max} (Py)/nm 356 (lg ϵ 4.74) and 663 (4.64). ¹H NMR (600.13 MHz, [D₅]Py) δ H ppm: 15.57–16.32 (16H, m, H_{Ph}), 17.52–18.11 (16H, m, H_{Ph}) and 19.29–21.70 (8H, m, H_{Ph}). IR (KBr): ν (cm^{–1}): 1282–1379 (C–O), 1379–1633 (γ pyrrole and pyrazine), 1513–1633 (C=O), 2850–2935 (st CH CH₃COO[–]), 3057 (st CH_{Ph}).

[2,3,9,10,16,17,23,24-Octaphenyl-1,4,8,11,15,18,22,25-octaazaphthalocyaninato]lutetium acetate (2f):

Approach A (i). A mixture of compound **1** (0.20 g, 0.71 mmol), Lu(OAc)₃ × 4H₂O (0.15 g, 0.36 mmol) and *p*-hydroquinone (0.16 g, 1.45 mmol) was taken in a glass tube. The resulting mixture was irradiated in a microwave oven (600 W) for 15 min. Then the reaction mixture was cooled to room temperature and

a MeOH–H₂O (20 : 1 v/v) mixture was added. The precipitate was filtered and washed with water, MeOH, and acetone. This yielded complex **2f** (0.13 g, 54%). MS (MALDI-TOF) *m/z*: 1457 ([M–OAc + DHB]⁺, 100%). UV-vis λ_{max} (Py)/nm 354 (lg ϵ 4.69) and 665 (4.56). ¹H NMR (400.13 MHz, [D₅]Py) δ H ppm: 7.66–7.69 (16H, m, H_{Ph}), 7.71–7.74 (16H, m, H_{Ph}) and 7.78 (8H, br., H_{Ph}). IR (KBr): ν (cm^{–1}): 1321–1446 (C–O), 1377–1633 (γ pyrrole and pyrazine), 1512–1633 (C=O), 2850–2933 (st CH CH₃COO[–]), 3054 (st CH_{Ph}).

Approach A (ii). A mixture of compound **1** (0.050 g, 0.18 mmol), Lu(OAc)₃ × 4H₂O (0.031 g, 0.08 mmol) and *p*-hydroquinone (0.040 g, 0.018 mmol) was heated at 200 °C in a glass tube, equipped with an air cooled condenser, for 15 min. Then the reaction mixture was cooled to room temperature and a MeOH–H₂O (20 : 1 v/v) mixture was added. The precipitate was filtered and washed with H₂O, MeOH, and acetone. This yielded complex **2f** (0.037 g, 60%). The characteristics were identical with those obtained by Approach A (i).

Approach B. Compound **4** (0.050 g, 0.044 mmol) and Lu(OAc)₃ × 4H₂O (0.038 g, 0.088 mmol) were refluxed in 3 mL *o*-dichlorobenzene (*o*-DCB) in the presence DBU (0.2 mmol) for 2 h. Then the reaction mixture was cooled to room temperature and a MeOH–H₂O (20 : 1, v/v) mixture was added. The precipitate was filtered and washed with water, MeOH, and acetone. This yielded complex **2f** (0.056 g, 91%). The characteristics were identical with those obtained by Approach A (i).

[2,3,9,10,16,17,23,24-Octaphenyl-1,4,8,11,15,18,22,25-octaazaphthalocyaninato]dilithium (3). A mixture of compound **1** (0.40 g, 1.42 mmol), MeOLi (0.11 g, 2.89 mmol) and *p*-hydroquinone (0.080 g, 0.73 mmol) was placed into a glass tube. The resulting mixture was irradiated in a microwave oven (600 W) for 15 min. Then the reaction mixture was cooled to room temperature and a MeOH–H₂O (20 : 1 v/v) mixture was added. The precipitate was filtered and washed with H₂O, MeOH, and acetone. This yielded complex **3** (0.31 g, 76%). MS (MALDI-TOF) *m/z*: 1132 ([M–2Li + 3H]⁺, 30%), 1154 ([M–2Li + Na + 2H]⁺, 100%), 1176 ([M–2Li + 2Na + H]⁺). UV-vis λ_{max} (Py)/nm 370 (lg ϵ 4.56) and 660 (4.66). IR (ZnSe): ν (cm^{–1}): 1377–1612 (γ pyrrole and pyrazine), 3062 (st CH_{Ph}).

2,3,9,10,16,17,23,24-Octaphenyl-1,4,8,11,15,18,22,25-octaazaphthalocyanine (4). Complex **3** (0.31 g, 0.27 mmol) was dissolved in polyphosphoric acid (30 ml) and stirred at 110 °C for 2 h. Then the mixture was cooled to room temperature, and distilled H₂O was added. Ammonium carbonate was added until neutral pH of the reaction mixture was reached. The precipitate was filtered and washed with H₂O, MeOH, and acetone. This yielded compound **4** (0.25 g, 82%). MS (MALDI-TOF) *m/z*: 1131 ([M + H]⁺, 100%). UV-vis λ_{max} (CHCl₃)/nm 363 (lg ϵ 3.98), 639 (4.56) and 672 (4.63). IR (ZnSe): ν (cm^{–1}): 1346–1637 (γ pyrrole and pyrazine), 3059 (st CH_{Ph}), 3288 (st NH).

Conclusions

Novel phenyl-substituted pyrazinoporphyrazine complexes of rare-earth elements (Y, Eu, Gd, Dy, Er, and Lu) were obtained in

high yields using a modified template approach and a multi-step synthesis involving formation of the porphyrazine ligand. The main feature of our protocol for the template synthesis was the use of *p*-hydroquinone as a reducing agent and the reaction medium at the same time. Target complexes were identified by high resolution MALDI-TOF mass-spectrometry, IR and NMR spectroscopy. The impact of the paramagnetic nature of lanthanide ions on the ^1H NMR spectra of the porphyrazine complexes was investigated for the first time. A downfield shift of the signals of phenyl protons for the europium and erbium complexes compared to diamagnetic ones has been demonstrated. An upfield shift of the signals of aromatic protons up to -26.88 ppm was observed for the dysprosium complex. Redox transitions in pyridine and UV-vis absorption spectra in solutions and films were characterized. In comparison with phenyl-substituted phthalocyanine complexes, a hypsochromic shift of the *Q* band of about 30 nm was observed. The electrochemical measurements revealed the strong electron withdrawing nature of the pyrazine fragments in octaphenyl-substituted pyrazinoporphyrazines compared to phthalocyanine analogues. A characteristic energy diagram was obtained for the erbium complex **2e** in a thin film and in poly(methyl acrylate) matrix. In poly(methyl acrylate) film, a polymeric matrix prevents strong aggregation of the porphyrazine molecules and allows energy levels for the monomeric form to be obtained. The results for erbium complex **2e** in poly(methyl acrylate) film are as follows: -4.1 eV for the LUMO level; -4.7 eV for the Fermi level; -4.5 , -5.9 , and -7.5 eV for additional energy levels. The accuracy of determination is at or below 0.1 eV.

Conflicts of interest

There are no conflicts to declare.

Acknowledgements

We are grateful for main financial support from the Russian Foundation for Basic Research (Grant No. 16-33-60005 and 18-33-00519). Investigation of optical properties was supported by the Russian Science Foundation (Grant 17-13-01197). Electrochemical investigations were supported by ERA.Net RUS Plus Plasmon ElectroLight and FWO funding (RFBR No. 18-53-76006 ERA). We also thank the Council under the President of the Russian Federation for State Support of Young Scientists and Leading Scientific Schools (Grants MK-3115.2018.3) and partial support from the framework of the State Assignment of 2019 (Theme 45.5 Creation of compounds with given physicochemical properties). Investigation of electro-physical properties was supported by the RFBR (Grant 16-07-00961). K. A. Drozdov and M. S. Kotova thank Prof. L. I. Ryabova for productive discussion of the electrophysical data.

References

- J. M. Fox, T. J. Katz, S. Van Elshocht, T. Verbiest, M. Kauranen, A. Persoons, T. Thongpanchang, T. Krauss and L. Brus, *J. Am. Chem. Soc.*, 1999, **121**, 3453–3459.
- M. Villano, V. Amendola, G. Sandonà, M. P. Donzello, C. Ercolani and M. Meneghetti, *J. Phys. Chem. B*, 2006, **110**, 24354–24360.
- D. Schlettwein, D. Woehrl, E. Karmann and U. Melville, *Chem. Mater.*, 1994, **6**, 3–6.
- P. Zimcik, M. Miletin, Z. Musil, K. Kopecky, L. Kubza and D. Brault, *J. Photochem. Photobiol., A*, 2006, **183**, 59–69.
- E. H. Mørkved, N. K. Afseth and P. Zimcik, *J. Porphyrins phthalocyanines*, 2007, **11**, 130–138.
- V. Novakova, M. Lásková, H. Vavříčková and P. Zimcik, *Chem. – Eur. J.*, 2015, **21**, 14382–14392.
- D. K. P. Ng and J. Jiang, *Chem. Soc. Rev.*, 1997, **26**, 433–442.
- V. E. Pushkarev, L. G. Tomilova and V. N. Nemykin, *Coord. Chem. Rev.*, 2016, **319**, 110–179.
- J. Jiang and D. K. P. Ng, *Acc. Chem. Res.*, 2009, **42**, 79–88.
- W. Cao, H. Wang, X. Wang, H. K. Lee, D. K. P. Ng and J. Jiang, *Inorg. Chem.*, 2012, **51**, 9265–9272.
- W. Cao, C. Gao, Y.-Q. Zhang, D. Qi, T. Liu, K. Wang, C. Duan, S. Gao and J. Jiang, *Chem. Sci.*, 2015, **6**, 5947–5954.
- H. Pan, L. Gong, W. Liu, C. Lin, Q. Ma, G. Lu, D. Qi, K. Wang and J. Jiang, *Dyes Pigm.*, 2018, **156**, 167–174.
- W. Liu, H. Pan, Z. Wang, K. Wang, D. Qi and J. Jiang, *Chem. Commun.*, 2017, **53**, 3765–3768.
- K. Wang, F. Ma, D. Qi, X. Chen, Y. Chen, Y.-C. Chen, H.-L. Sun, M.-L. Tong and J. Jiang, *Inorg. Chem. Front.*, 2018, **5**, 939–943.
- C. Yuxiang, L. Chao, M. Fang, Q. Dongdong, L. Qingyun, S. Hao-Ling and J. Jianzhuang, *Chem. – Eur. J.*, 2018, **24**, 8066–8070.
- E. A. Kuzmina, T. V. Dubinina, A. V. Zasedatelev, A. V. Baranikov, M. I. Makedonskaya, T. B. Egorova and L. G. Tomilova, *Polyhedron*, 2017, **135**, 41–48.
- H. Wang, W. Cao, T. Liu, C. Duan and J. Jiang, *Chem. – Eur. J.*, 2013, **19**, 2266–2270.
- N. Kobayashi, J. Rizhen, S.-I. Nakajima, T. Osa and H. Hino, *Chem. Lett.*, 1993, 185–188.
- S. Tomachynskiy, S. Korobko, L. Tomachynski and V. Pavlenko, *Opt. Mater.*, 2011, **33**, 1553–1556.
- T. A. Lebedeva, V. P. Kulinich, G. P. Shaposhnikov, S. V. Efimova, A. B. Korzhenevskii and O. I. Koifman, *Russ. J. Gen. Chem.*, 2007, **77**, 1944–1950.
- T. V. Dubinina, K. V. Paramonova, S. A. Trashin, N. E. Borisova, L. G. Tomilova and N. S. Zefirov, *Dalton Trans.*, 2014, **43**, 2799–2809.
- T. V. Dubinina, A. D. Kosov, E. F. Petrusovich, S. S. Maklakov, N. E. Borisova, L. G. Tomilova and N. S. Zefirov, *Dalton Trans.*, 2015, **44**, 7973–7981.
- E. M. Bauer, C. Ercolani, P. Galli, I. A. Popkova and P. A. Stuzhin, *J. Porphyrins phthalocyanines*, 1999, **3**, 371–379.
- H. W. Rothkopf, D. Wöhrle, R. Müller and G. Kößmehl, *Chem. Ber.*, 1975, **108**, 875–886.
- E. A. Kuzmina, T. V. Dubinina, N. E. Borisova and L. G. Tomilova, *Macroheterocycles*, 2017, **10**, 520–525.
- İ. Gürol, V. Ahsena and Ö. Bekaroğlu, *J. Chem. Soc., Dalton Trans.*, 1994, 497–500, DOI: 10.1039/DT9940000497.

- 27 S. V. Kudrevich and J. E. van Lier, *Coord. Chem. Rev.*, 1996, **156**, 163–182.
- 28 K. Nakamoto, *Infrared and Raman Spectra of Inorganic and Coordination Compounds*, John Wiley and Sons Inc, New York, Chichester, Brisbane, Toronto, Singapore, 4th edn, 1986.
- 29 T. V. Dubinina, P. I. Tychinsky, N. E. Borisova, V. I. Krasovskii, A. S. Ivanov, S. V. Savilov, S. S. Maklakov, M. V. Sedova and L. G. Tomilova, *Dyes Pigm.*, 2018, **156**, 386–394.
- 30 N. Jiazan, S. Feng, L. Zhenxiang and Y. Shaoming, *Inorg. Chim. Acta*, 1987, **139**, 165–168.
- 31 I. V. Nefedova, Y. G. Gorbunova, S. G. Sakharov and A. Y. Tsivadze, *Russ. J. Inorg. Chem.*, 2005, **50**, 165–173.
- 32 V. E. Pushkarev, M. O. Breusova, E. V. Shulishov and Y. V. Tomilov, *Russ. Chem. Bull.*, 2005, **54**, 2087–2093.
- 33 J. Jiang, T. C. W. Mak and D. K. P. Ng, *Chem. Ber.*, 1996, **129**, 933–936.
- 34 H. Konami, M. Hatano and A. Tajiri, *Chem. Phys. Lett.*, 1989, **160**, 163–167.
- 35 N. Kobayashi, S.-i. Nakajima, H. Ogata and T. Fukuda, *Chem. – Eur. J.*, 2004, **10**, 6294–6312.
- 36 T. V. Dubinina, S. A. Trashin, N. E. Borisova, I. A. Boginskaya, L. G. Tomilova and N. S. Zefirov, *Dyes Pigm.*, 2012, **93**, 1471–1480.
- 37 K. Seeger, *Semiconductor Physics*, Springer, Berlin, Heidelberg, 2004.
- 38 J. S. Blakemore, *Solid State Physics*, Cambridge University Press, 1985.
- 39 T. Basova, A. G. Gürek, V. Ahsen and A. K. Ray, *Org. Electron.*, 2007, **8**, 784–790.
- 40 T. Nyokong, in *Functional Phthalocyanine Molecular Materials*, ed. J. Jiang, Springer Berlin Heidelberg, Berlin, Heidelberg, 2010, pp. 45–87, DOI: 10.1007/978-3-642-04752-7_2.
- 41 P. Zhu, N. Pan, R. Li, J. Dou, Y. Zhang, D. Y. Y. Cheng, D. Wang, D. K. P. Ng and J. Jiang, *Chem. – Eur. J.*, 2005, **11**, 1425–1432.
- 42 P. Zhu, F. Lu, N. Pan, D. P. Arnold, S. Zhang and J. Jiang, *Eur. J. Inorg. Chem.*, 2004, 510–517.
- 43 M. P. Donzello, R. Agostinetti, S. S. Ivanova, M. Fujimori, Y. Suzuki, H. Yoshikawa, J. Shen, K. Awaga, C. Ercolani, K. M. Kadish and P. A. Stuzhin, *Inorg. Chem.*, 2005, **44**, 8539–8551.
- 44 C. Bergami, M. P. Donzello, F. Monacelli, C. Ercolani and K. M. Kadish, *Inorg. Chem.*, 2005, **44**, 9862–9873.
- 45 M. P. Donzello, D. Dini, G. D'Arcangelo, C. Ercolani, R. Zhan, Z. Ou, P. A. Stuzhin and K. M. Kadish, *J. Am. Chem. Soc.*, 2003, **125**, 14190–14204.
- 46 A. Ghosh, P. G. Gassman and J. Almloef, *J. Am. Chem. Soc.*, 1994, **116**, 1932–1940.
- 47 A. Lee, D. Kim, S. H. Choi, J. W. Park, J. Y. Jaung and D. H. Jung, *Mol. Simul.*, 2010, **36**, 192–198.
- 48 M. Hamdoush, S. S. Ivanova, O. I. Koifman, M. Kos'kina, G. L. Pakhomov and P. A. Stuzhin, *Inorg. Chim. Acta*, 2016, **444**, 81–86.
- 49 K. Ohta, T. Watanabe, T. Fujimoto and I. Yamamoto, *J. Chem. Soc., Chem. Commun.*, 1989, 1611–1613, DOI: 10.1039/C39890001611.
- 50 M. P. Donzello, Z. Ou, D. Dini, M. Meneghetti, C. Ercolani and K. M. Kadish, *Inorg. Chem.*, 2004, **43**, 8637–8648.
- 51 L. E. Hinkel, G. O. Richards and O. Thomas, *J. Chem. Soc.*, 1937, 1432–1437, DOI: 10.1039/JR9370001432.